Precise measurement of pion-bump structure using future MeV gamma-ray detectors

Jiahao Liu,[1,2,3] Bing Liu,[1,2,3] and Ruizhi Yang[1,2,3,*]

[1]*Deep Space Exploration Laboratory, Hefei 230088, China*
[2]*CAS Key Laboratory for Research in Galaxies and Cosmology, Department of Astronomy, School of Physical Sciences, University of Science and Technology of China, Hefei, Anhui 230026, China*
[3]*School of Astronomy and Space Science, University of Science and Technology of China, Hefei, Anhui 230026, China*

(Received 1 March 2024; accepted 20 August 2024; published 13 September 2024)

The pion-bump structure in the γ-ray spectrum is a direct proof for the hadronic origin of the γ rays, and thus the decisive evidence for the acceleration of hadronic cosmic rays in astrophysical objects. However, the identification of such a spectral feature is limited by the resolution and energy coverage of current γ-ray instruments. Furthermore, there are unavoidable bremsstrahlung emissions from secondary and primary electrons, which may dominate the γ-ray emission below the pion-bump. Thus, the study of this γ-ray emission component can provide unique information on the acceleration and confinement of high-energy particles. In this paper, we studied the predicted γ-ray spectrum assuming both hadronic or leptonic origin in mid-aged supernova remnants W44, we discuss the detection potential of future MeV missions on these emissions and possible implications.

DOI: 10.1103/PhysRevD.110.063026

I. INTRODUCTION

The origin of cosmic rays (CRs) is one of the most fundamental questions in modern astrophysics. Supernova remnants (SNRs) are regarded as the most promising acceleration sites of CRs (see, e.g., [1]). Thus, they are also prime targets in γ-ray emissions in both GeV and TeV energy ranges [2,3]. The origin of high-energy γ rays from SNRs is either from the inverse Compton (IC) scattering of relativistic electrons or from the pion-decay process in the inelastic scatterings of CR protons with ambient gas, while the latter is regarded as a strong proof that SNRs can accelerate CRs. However, the discrimination of leptonic and hadronic scenarios is not easy, since in the energy range above GeV both mechanisms can produce the power-law spectra as observed. One distinct spectral feature of the hadronic scenario is the so-called "pion bump," which is a sharp low-energy spectral cutoff due to the kinematics of the neutral pion-decay process.

AGILE and Fermi-LAT Collaborations reported the discovery of pion bumps in midaged SNR W44 and IC 443, which is regarded as decisive evidence that SNRs do accelerate hadronic CRs [4,5]. However, later studies have argued that the observed feature can also be attributed to the bremsstrahlung of electrons [6], especially taking into account that the electrons in the interstellar medium (ISM) also reveal a low-energy break at several GeV [7]. The observed low-energy break in both scenarios is most evident in the energy range between 10 and 100 MeV. Because of the limited sensitivity of current γ-ray instruments in this energy range, it is rather difficult to distinguish the two scenarios. Furthermore, even in the hadronic scenario, in which the GeV γ-ray emission are dominated by the pion-decay process, there are inevitably accompanied primary electrons accelerated at the same site, as well as the secondary electrons produced by the decay of charged pions in the inelastic collision of CR protons with ambient gas. These electrons can produce γ rays in the same environment via bremsstrahlung and may dominate the γ-ray emissions below the pion bump. Thus, the measurement of the γ-ray emissions below the pion bump can be used to study the physical conditions of the accelerators, such as the e/p ratio and particle confinement in the vicinity [8].

In this paper, we will study the possible advance in the detection of the pion bump in one of the most suitable sites for such kind of study, the midage SNR W44, using the next-generation MeV γ-ray detectors. The paper is organized as follows. In Sec. II, we briefly introduce the SNR W44 and the current γ-ray observations; we then calculate the γ-ray flux in the MeV band assuming either the γ rays are produced in the pion-decay process (hadronic scenario) or bremsstrahlung (leptonic scenario). Next, in Sec. III, we calculate the γ-ray emissions from primary/secondary electrons in the context of hadronic scenarios. Then, in Sec. IV, we estimate the detection ability of next-generation

[*]Contact author: yangrz@ustc.edu.cn

MeV detectors in this energy range. Finally, we discuss the possible implications of our calculation in Sec. V.

II. GAMMA RAYS FROM SNR W44

W44 (G034.7-00.4) is an old mixed-morphology SNR that has a radio continuum shell filled with thermal x-ray emission from the shock-heated gas. A pulsar wind nebula associated with pulsar PSR B1853 + 01 is also embedded within the SNR [9]. The distance to W44 is considered to be about 3 kpc according to the HI observations [10] and the detection of OH 1720 MHz maser spots implies the interaction between the SNR and the adjacent giant molecular cloud [11]. High-energy γ rays possibly associated with W44 were first detected by EGRET [12]. Then years later, AGILE and Fermi Collaborations reported the characteristic pion-decay signature from W44 successively [4,5]. Recently, a more detailed study performed by Peron *et al.* [6], which also preferred the hadronic origin of the γ rays associated with W44, still cannot exclude the possible interpretation of radiation by electron bremsstrahlung due to the systematic uncertainties. In this work, we take W44 as a typical case to study the ability of future MeV telescopes to distinguish the pion-decay emission from the bremsstrahlung emission.

First, we refitted the γ-ray spectral energy distribution (SED) (as shown in Fig. 1) from the SNR W44 derived in [6] with the NAIMA package [13]. This Python package offers functionalities for calculating γ-ray cross sections and likelihood fitting of the CR spectrum based on the observed γ-ray spectrum. Here, we assumed two different origins of the γ-ray emission, interactions of accelerated protons (hadronic scenario) and nuclei with the surrounding gas and bremsstrahlung from electrons (leptonic scenario).

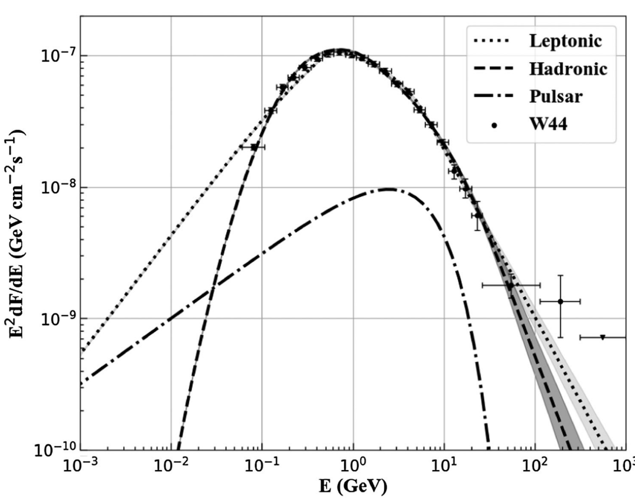

FIG. 1. SED of γ rays from W44. The lines and shaded areas show the modeled flux and 1σ uncertainty of each scenario. The dash-dotted line shows the hypothetical spectrum of the pulsar PSR B1853 + 01. The data points show the observed SED derived from Fermi Pass8 data [6].

There should also be IC emission from the same population of electrons that produce the radio/x-ray emission through synchrotron. However, in this case, the electrons producing 10–100 MeV γ rays through IC scattering of optical/UV photons (dominant in this energy range) should have a Lorentz factor $\Gamma^2 \sim 10^7$–10^8. The corresponding synchrotron frequency of these electrons can be estimated as $1.3\ \Gamma^2(B/1\ \mu\mathrm{G})$ Hz. Assuming $B \sim 3\ \mu$G, the synchrotron frequency will be 0.1–1 GHz. We also note that the energy density of the 3 μG magnetic field is about 0.4 eV/cm^3, which is similar to the energy density of optical/UV photon fields in the interstellar radiation field. Thus, the energy flux of IC in 10–100 MeV should be similar to the synchrotron energy flux at 0.1–1 GHz, which is 10^{-15} erg/s/cm^2, again much smaller than the flux we considered in our model and the sensitivity of next-generation MeV instruments. Of course, the magnetic field can be much larger, but in this case, the IC flux should be even smaller. We conclude that the IC contribution is not significant and will not consider it in the following parts of the article. Furthermore, the current discrimination is based on the broken power-law model of both the electron and proton spectra. This model is also justified by ionization cooling of low-energy protons/electrons or by injection. However, it remains unclear whether there exists additional spectral structures at even lower energies, as no detections have been made in this energy range thus far. Therefore, we currently maintain the assumption of a broken power-law model for both the electron and proton spectra in our calculations. We set the distribution of the parent protons or electrons as a broken power law of momentum,

$$f(p) = \begin{cases} A(p/p_0)^{-\alpha_1} & : p < p_\mathrm{b}, \\ A(p_\mathrm{b}/p_0)^{\alpha_2-\alpha_1}(p/p_0)^{-\alpha_2} & : p > p_\mathrm{b}. \end{cases} \tag{1}$$

In Eq. (1), p_b is the break momentum, A is the model amplitude at the break momentum, $p_0 = 10\ \mathrm{GeV}/c$, α_1 and α_2 are the power-law index for $p < p_\mathrm{b}$ and $p > p_\mathrm{b}$, respectively. A low-energy cutoff at $p^e_\mathrm{min} = 600\ \mathrm{MeV}/c$ was also added to the distribution function of the electrons in the leptonic scenario. The dashed line shows the fitted γ-ray emission in the hadronic scenario, and the dotted line shows the γ-ray spectrum obtained in the leptonic scenario. Meanwhile, the shaded area indicates the range of their 1σ uncertainty. The fitted parameters for the distribution of protons and electrons in the two scenarios are shown in Table I. We found that with these parameters both leptonic and hadronic scenarios can explain the observed GeV SEDs, but in the MeV band, the flux can be different by orders of magnitude due to sharp spectral cutoff in the pion-decay γ-ray spectrum. Such differences can provide conclusive discrimination on these two scenarios with the observations in the MeV band.

In addition, the pulsar PSR B1853 + 01 [9] can also be a potential γ-ray emitter. The 95% upper limit of the γ-ray

TABLE I. Parameters of the particle distribution in different scenarios.

Scenario	α_1	α_2	p_b (GeV/c)
Hadronic	2.44 ± 0.03	3.78 ± 0.15	35.5 ± 4.1
Leptonic	2.28 ± 0.05	3.37 ± 0.08	6.1 ± 0.8

emission from the pulsar over 100 MeV has been calculated to be 1.6×10^{-7} photons $\mathrm{cm}^{-2}\,\mathrm{s}^{-1}$ [14]. The spin-down luminosity of PSR B1853 + 01 is estimated as 4.3×10^{35} erg/s [15], assuming ∼10% of the spin-down power is emitted in γ rays and, given the distance of 2.2 kpc, the γ-ray flux of the pulsar is estimated to be 3×10^{-5} MeV/cm^2/s, which is roughly consistent with the upper limit from Fermi-LAT. If we further assume that the spectrum of the γ-ray emission from the pulsar follows a power law with an exponential cutoff, characterized by a typical spectral index of −1.5 and a break energy of 5 GeV [16], we then extrapolate the γ-ray flux down to 1 MeV assuming a total energy flux of 3×10^{-5} MeV/cm^2/s in the γ-ray band. This hypothetical spectrum is shown by the dash-dotted line in Fig. 1, which indicates that the pulsar can potentially contribute significantly to the MeV γ-ray emission. Because of the small distance of PSR B1853 + 01 and W44 it would be difficult to resolve the pulsar and the SNR. However, in this case, the pulsed emission can dominate the hadronic emission below dozens of MeV, which can be measured by future MeV observations.

III. CONTRIBUTION FROM PRIMARY AND SECONDARY ELECTRONS IN HADRONIC SCENARIO

In a hadronic scenario, the process $pp \to \pi^0 \to 2\gamma$ dominates the γ-ray production. However, even in the hadronic scenario, there will be inevitable primary electrons accelerated at the same site of the CR protons, as well as secondary electrons produced accompanying the pion-decay γ rays. These primary and secondary electrons can also contribute to the overall γ-ray radiation, which can be even more significant below 100 MeV. Following the method of [8], we estimated the contribution from primary and secondary electrons to the γ-ray emission.

We first discuss the evolution of relativistic particles. In a given volume, this is given by the kinetic equation (see, e.g., [17])

$$\frac{\partial N}{\partial t} = \frac{\partial}{\partial E}(PN) - \frac{N}{\tau_{\mathrm{esc}}} + Q, \tag{2}$$

where $P = P(E) = -\frac{dE}{dt}$ is the energy loss rate and τ_{esc} is the characteristic escape time. Neglecting the particle escape from the γ-ray production region, we can give upper limits on the contribution of secondary electrons to the overall γ-ray flux.

For continuous injection $Q(E, t) = Q(E)$, the solution of kinetic equation becomes

$$N(E, t) = \frac{1}{P(E)} \int_E^{E_0} Q(E) dE, \tag{3}$$

where E_0 is found by solving $t = \int_E^{E_0} \frac{dE}{P(E)}$, which is the characteristic equation for the given epoch, t.

The cooling of electrons is mainly caused by ionization losses, synchrotron, bremsstrahlung, and IC radiation. The energy loss rate of ionization P_{ion} is proportional to gas density and scales as $1/\beta$ at low energies between 1 MeV and 1 GeV, where $\beta = v/c$. A convenient analytical presentation for the ionization losses can be found in [18]. In the case of W44, we set the gas density $n = 10\ \mathrm{cm}^{-3}$ [6], the magnetic fields $B = 3\ \mu\mathrm{G}$, and the age $T = 10^{12}$ s. The spectra of protons and electrons in different scenarios in Sec. II are the evolved spectra derived from the observed γ-ray data. As the break energy is as high as 35 GeV, the spectrum of protons in the MeV range is assumed to be power laws in momentum with the same index α_1,

$$Q(E) = \frac{N(p_0)}{\beta c} \left(\frac{p}{p_0}\right)^{-\alpha_1}, \tag{4}$$

where p is the proton momentum, and p_0 is the reference point taken to be 10 GeV/c.

The interstellar radiation fields are assumed to comprise three components: the 2.7 K cosmic microwave background, whose energy density is $0.24\ \mathrm{eV\,cm^{-3}}$, the optical/UV field modeled as a gray-body component with an energy density of $2\ \mathrm{eV\,cm^{-3}}$ and temperature of 5000 K, and the infrared component, which is modeled as a gray-body component with an energy density of $1\ \mathrm{eV\,cm^{-3}}$ and a temperature of 100 K [8]. For the primary electrons, it was assumed that their injection spectrum has the same shape as that of the primary protons. We regulated the injection spectrum of primary electrons by applying a constant e/p ratio (k_{ep}) at 10 GeV. By calculating Eq. (3), we derived the spectrum of primary electrons after time evolution, which is shown in Fig. 2. As for the secondary electrons, we assumed a constant distribution of parent protons to derive their injection spectrum. Then we calculated the spectrum after the time revolution by calculating Eq. (3), which is shown in Fig. 2. We found that the contribution of secondary electrons can be ignored when compared to the primary electrons. Thus, only the contribution of primary electrons was considered for further calculation in Sec. IV. However, this only applies to the case of W44. For other sources, due to differences in gas density, evolution time, and other factors, secondary electrons may still make a significant contribution [8].

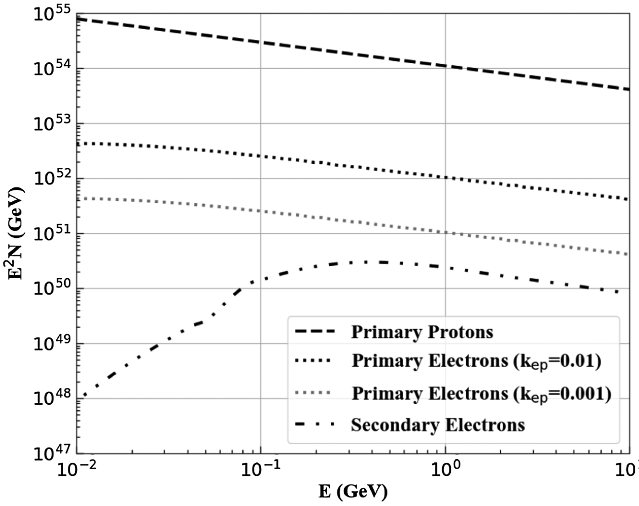

FIG. 2. Estimated energy distributions of the number of different particles after time revolution in the hadronic scenario. The gas density was set to be $n = 10\ \mathrm{cm}^{-3}$ and the age was set to be $T = 10^{12}$ s.

IV. DETECTABILITY OF NEXT-GENERATION MEV INSTRUMENTS

Based on the calculations in Sec. II, the γ-ray spectra produced in the hadronic and leptonic scenarios can exhibit significant differences in the MeV energy range. Therefore, we have estimated the future observational results of a next-generation MeV γ-ray telescope, MeGaT, to evaluate its observational performance and determine whether its observations can distinguish between the radiation mechanisms that produce the γ-ray from W44. The MeGaT project is a planned MeV space γ-ray telescope in China. The main design concept of MeGaT is to use a time projection chamber as the tracking detector together with a high-resolution calorimeter in the bottom. MeGaT has a wide energy range of 0.3–100 MeV, covering both the Compton scattering and pair production regime. In Compton scattering, the point spread function (PSF) is determined equivalently by the two angular resolutions of the elevation and azimuth in general. The latter is a function of the scatter plane deviation (SPD). For a good PSF, the improvement of the SPD is far more important considering the present resolution. MeGaT used a gaseous detector as the tracking detector, which can largely improve the SPD. Current simulations indicate that MeGaT can achieve a 0.5° PSF at approximately 100 MeV and a 2° PSF at approximately 1 MeV. The sensitivity of MeGaT is estimated to be around $3\times10^{-12}\ \mathrm{erg\,cm^{-2}\,s^{-1}}$ ($\sim2\times10^{-7}\ \mathrm{MeV\,cm^{-2}\,s^{-1}}$) at 1 MeV, using the reconstruction of Compton scattering, and around $2\times10^{-12}\ \mathrm{erg\,cm^{-2}\,s^{-1}}$ ($\sim1\times10^{-7}\ \mathrm{MeV\,cm^{-2}\,s^{-1}}$) at 100 MeV, using the reconstruction of pair production. Detailed information about MeGaT, like the instrument response function (IRF) and sensitivity curve, will be presented in a dedicated work. In this article, we assumed that MeGaT has an effective area of 100 cm^2, and its angular resolution was taken to be 1°, which is consistent with current predictions. Since the full IRF with energy dependence is not yet available, in the current work, as a schematic study, we did not take into account the energy dependence of IRFs. The details of the use of these parameters during calculation are described later in this section.

Utilizing the fitted particle distributions obtained in Sec. II, we can calculate the γ-ray flux distributions with the NAIMA package in the MeV energy range corresponding to the two scenarios, respectively. Although W44 is an extended source, its size is still much smaller than the PSFs of the MeV instruments. So we applied the "aperture photometry" method and used all the photon counts in a disk region centered at W44 with a radius of the PSF (1°) of MeGaT. We also estimated the diffuse background flux in the direction of W44 by integrating the known MeV energy range data in this disk region. For energy between 0.5 and 8.0 MeV, we adopted the diffuse Galactic emission reanalyzed by [19] based on the observation of spectrometer aboard INTEGRAL using GALPROP [20] models in a 95° × 95° region around the Galactic Center. For energy over 50 MeV, we utilized the Fermi-LAT interstellar emission model [21], which was based on the first nine years of Fermi-LAT data. A fits version of this model, `gll_iem_v07.fits`, is accessible on the Fermi Science Support Center website [22]. Specially, we calculated the contribution of point sources in the same region by 14 years of the Fermi-LAT data using the Fermitools from Conda distribution [23]. We generated the γ-ray counts maps and the exposure maps in different energy ranges to calculate the total flux in the reference region and found that the results were similar to that from the Fermi interstellar emission model. However, in a larger integration area, 10° for example, the contribution of point sources would be non-negligible due to the crowded source distribution on the Galactic plane. The total flux would be 2–3 times higher than that of the diffuse background. Thus, the angular resolution can be very important for such kind of study. The distribution of background flux in the whole energy range was then determined by cubic extrapolation in logarithmic space. Given the effective area (A_{eff}) of different instruments, we calculated the total counts of γ rays from W44 and the diffuse background in the 1–100 MeV energy range that could be observed within 2 months of observational time (T_{obs}). We divided the data from 1 to 100 MeV into four energy bins. We estimated the possible data counts of each bin assuming an exposure of 2 months by

$$N_{\mathrm{counts}} = \int_{E_{\mathrm{lower}}}^{E_{\mathrm{upper}}} F(E) T_{\mathrm{obs}} A_{\mathrm{eff}}(E) dE, \tag{5}$$

where $F(E)$ is the theoretical differential flux calculated in Sec. II, T_{obs} is the observational time, $A_{\mathrm{eff}}(E)$ is the effective area of the telescope, and E_{lower} and E_{upper} are the lower and upper bond of the energy bin, respectively. In most of the energy range, the theoretical prediction of the γ-ray flux in the hadronic scenario is less than that of the leptonic scenario by more than 1 order of magnitude. Therefore, we only estimated the predicted counts of γ rays in the leptonic scenario here. The results of the γ-ray counts are shown in Table II. We then assumed a Poisson distribution of the data and calculated the uncertainty σ of the data by

$$\sigma = \sqrt{N_{\mathrm{total}}} = \sqrt{N_{\mathrm{signal}} + N_{\mathrm{bkg}}}, \tag{6}$$

where N_{total} is the sum of the predicted γ-ray counts of signal (N_{signal}) and background (N_{bkg}). We also calculated the significance (S) of the data by

$$S = \frac{N_{\mathrm{signal}}}{\sqrt{N_{\mathrm{signal}} + N_{\mathrm{bkg}}}}. \tag{7}$$

As the counts of both signal and background are proportional to T_{obs}, it naturally follows that the significance S should be proportional to $\sqrt{T_{\mathrm{obs}}}$. The results are shown in Table II and Fig. 3, which indicate that a T_{obs} of 2 months would be adequate for the data to reach enough significance.

To distinguish whether the γ-ray emission originated in a leptonic or hadronic scenario, we calculated the 3σ upper limit assuming the γ rays were produced via the pion-decay mechanism

$$F_{\mathrm{up}} = \frac{N_{\mathrm{signal}} + 3\sqrt{N_{\mathrm{signal}} + N_{\mathrm{bkg}}}}{A_{\mathrm{eff}}(E_{\mathrm{mid}})T_{\mathrm{obs}}(E_{\mathrm{upper}} - E_{\mathrm{lower}})}, \tag{8}$$

where F_{up} is the 3σ upper limit of the measured γ-ray flux, and $E_{\mathrm{mid}} = \sqrt{E_{\mathrm{upper}}E_{\mathrm{lower}}}$ is the central energy of the energy bin. The results are shown in Fig. 3. As shown in the figure, we can easily distinguish between the two scenarios after 2 months of observation.

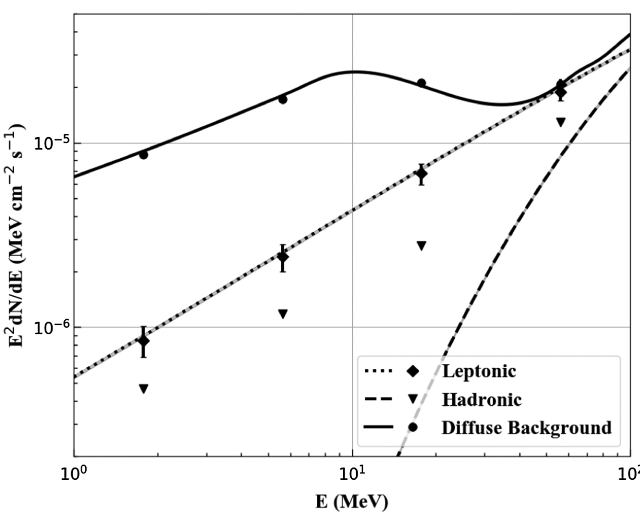

FIG. 3. Estimated SED of future MeV γ-ray observations of W44 in different scenarios. This observation result adopted the instrument parameters of MeGaT, and T_{obs} was taken to be 2 months. The lines and shaded areas show the theoretical flux and 1σ uncertainty of each scenario. The data points and error bars show the derived flux and 1σ uncertainty of the four energy bins. The inverted triangles show the 3σ upper limit of the flux of γ-ray emission in the pion-decay scenario.

TABLE II. Predicted counts of future MeGaT observation for γ-ray in the leptonic scenario ($T_{\mathrm{obs}} = 2$ months).

log(E/MeV)	N_{signal}	N_{bkg}	S (σ)
0.0–0.5	306	3099	5.24
0.5–1.0	274	1954	5.80
1.0–1.5	245	763	7.72
1.5–2.0	213	236	10.05

TABLE III. Predicted counts of future MeGaT observation for γ rays in the hadronic scenario ($T_{\mathrm{obs}} = 2$ months). The counts of the diffuse background is the same as Table II.

	N_{signal}		S (σ)	
log(E/MeV)	e/p = 0.01	e/p = 0.001	e/p = 0.01	e/p = 0.001
0.0–0.5	2676	268	35.21	4.62
0.5–1.0	583	60	11.57	1.34
1.0–1.5	137	28	4.57	1.00
1.5–2.0	116	95	6.19	5.23

Additionally, the MeV γ-ray observation can put limits on the e/p ratio in the hadronic scenario. Using the spectrum of primary electrons derived in Sec. III, we calculated the γ-ray contribution from the bremsstrahlung of these electrons and used the same method to calculate the telescope observation results in four energy bins. We assumed two uniform e/p ratios, 0.01 and 0.001, and applied similar calculations, respectively. The results are shown in Table III and Fig. 4. It can be seen that the change in the e/p ratio can significantly influence the MeV γ-ray spectrum, especially in lower energy. Because of the unavoidable contribution from primary electrons in the hadronic scenario, it would become more difficult to distinguish it from the leptonic model. However, compared with the pure leptonic scenario, the hadronic scenario with primary electrons would introduce a distinct "valley" structure in the spectrum just below the pion bump (at dozens of MeV), as shown in Fig. 4. Such feature can also be recognized with an exposure of several months.

V. DISCUSSION

The pion-decay bump is decisive proof for the acceleration of CR protons in astrophysical objects. Such feature

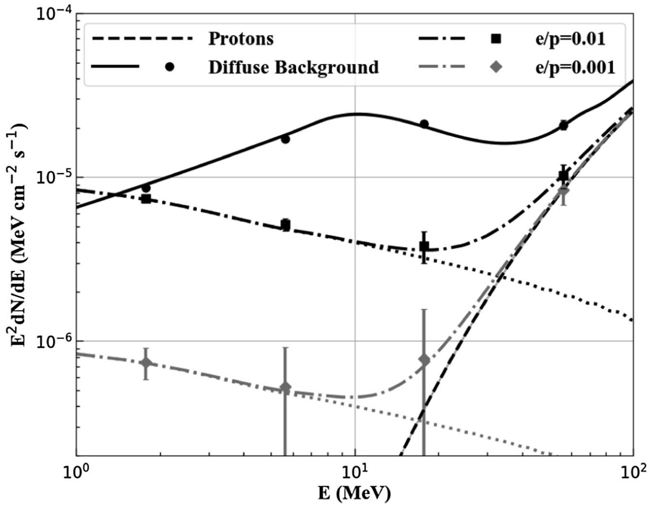

FIG. 4. Estimated SED of future MeV γ-ray observations of W44 in hadronic scenario. This observation result adopted the instrument parameters of MeGaT, and T_{obs} was taken to be 2 months. The lines show the theoretical γ-ray flux from different origins. Specially, the black and gray dotted line shows the flux from the bremsstrahlung of primary electrons and the chain lines show the summed flux from both primary electrons and primary protons. The data points and error bars show the derived flux and 1σ uncertainty of the four energy bins.

is most significant below 100 MeV and thus is an ideal scientific objective for next-generation MeV detectors. In this paper, we chose SNR W44 as an example to investigate the possible MeV γ-ray emission around and below the pion-decay bump. We found that, although the current γ-ray observations can be explained by both pion-decay and Bremsstrahlung processes, the future observations at about 10 MeV can distinguish these two mechanisms significantly with a reasonable exposure.

We also explored alternative future MeV detectors such as the Compton spectrometer and imager (COSI) [24]. Given its angular resolution of 4.1° at 0.511 MeV and 2.1° at 1.809 MeV, we found that no significant number of other point sources within the region would fall within the angular resolution. The continuum sensitivity of COSI is about 3×10^5 MeV cm^{-2} s^{-1} at 1 MeV and rises fast with energy above 1 MeV for the 2 yr survey, which makes it quite difficult to detect MeV emissions from W44.

Furthermore, even in the pure hadronic case, where the GeV γ rays are all produced by the pion-decay process, there are inevitable primary electrons accelerated at the same site where CR protons are accelerated and also the secondary electrons from the decay of charged pions produced by the inelastic scattering of CR protons with the ambient gas. These primary and secondary electrons will also produce γ rays via Bremsstrahlung. The γ rays from these electrons are negligible at the GeV energy range but can dominate below the pion-decay bump. In the case of W44, due to the relatively young age of this system, the contribution from secondary electrons is expected to be much smaller than those from primary electrons. Thus, the precise measurement of the spectrum below the pion-decay bump in this source would provide unique information on the injected primary electron spectrum; it especially can provide a direct measurement of the e/p ratio in this accelerator, which may provide important information to understand the particle acceleration as well as the origin of the anomalous electron spectrum observed locally [25–28].

On the other hand, as calculated in Yang *et al.* [8], in the case when $n \times T$ is as large as 10^{15} cm^{-3} s the bremsstrahlung γ rays from secondary electrons can also contribute significantly, where n is the ambient gas density and T is the confinement time of the CR particles. Such conditions can be realized in dense regions near older accelerators. The measurement of MeV γ rays in these environments can then provide information on the particle confinement near the accelerators, which are believed to be more effective than in the ISM [29].

To conclude, the MeV observation is a unique tool for probing CR-related science. For the specific case of SNR W44, in which the pion-decay bump feature was detected for the first time, the dedicated MeV investigations using future MeV detectors can significantly improve the ability to distinguish the pion-decay bump from the Bremsstrahlung emissions of CR electrons. Furthermore, in case the pion-decay bump is confirmed, the precise observation of the γ-ray spectrum below the pion-decay bump can provide a direct measurement of the e/p ratio in the accelerated CR in W44. Even after taking into account the diffuse background in this energy range, a marginal exposure of 2 months would be enough for such kind of study for planned MeV detectors such as MeGat and AMEGO [30]. For other older accelerators with higher ambient density, the MeV observations can also provide clues on the particle confinement near the accelerators.

MeV γ-ray astronomy is an important window for CR study. For example, the direct measurement of MeV deexcitation nuclear lines induced by the inelastic scattering of low-energy CRs (LECRs) with the ambient gas is probably the best way to study LECRs [31,32]. The most accepted site for very high-energy and ultrahigh-energy CR (UHECR) production is related to the supermassive black holes and associated powerful jet [33,34]; in this dense environment, the produced UHECRs will interact with the ambient medium and produce electromagnetic radiations. Because of the high opacity and effective pair production, only MeV γ rays can escape and potentially be detected. Thus, MeV observations are also crucial in understanding the origin of UHECRs [35]. In this paper, in addition to the above two aspects, we showed that the MeV observations can also provide decisive criteria on the pion-decay nature of γ-ray emissions in the potential accelerator and can be also used to study the e/p ratio in the accelerator as well as the confinement of CRs near the accelerators. These measurements can thus provide fresh information to understand the acceleration of CRs and could be another important scientific objective for future MeV astronomy.

ACKNOWLEDGMENTS

R. Y. is supported by the NSFC under Grant No. 12041305 and the national Youth Thousand Talents program in China. B. L. acknowledges the support from the NSFC under Grant No. 12103049.

[1] P. Blasi, The origin of galactic cosmic rays, Astron. Astrophys. Rev. **21**, 70 (2013).

[2] F. Acero, M. Ackermann, M. Ajello *et al.*, The first Fermi LAT supernova remnant catalog, Astrophys. J. Suppl. Ser. **224**, 8 (2016).

[3] H. Abdalla, A. Abramowski *et al.* (H.E.S.S. Collaboration), The H.E.S.S. Galactic plane survey, Astron. Astrophys. **612**, A1 (2018).

[4] A. Giuliani, M. Cardillo, M. Tavani *et al.*, Neutral pion emission from accelerated protons in the supernova remnant W44, Astrophys. J. **742**, L30 (2011).

[5] M. Ackermann, M. Ajello, A. Allafort *et al.*, Detection of the characteristic pion-decay signature in supernova remnants, Science **339**, 807 (2013).

[6] G. Peron, F. Aharonian, S. Casanova, R. Zanin, and C. Romoli, On the gamma-ray emission of W44 and its surroundings, Astrophys. J. **896**, L23 (2020).

[7] A. W. Strong, E. Orlando, and T. R. Jaffe, The interstellar cosmic-ray electron spectrum from synchrotron radiation and direct measurements, Astron. Astrophys. **534**, A54 (2011).

[8] R.-z. Yang, E. Kafexhiu, and F. Aharonian, Exploring the shape of the γ-ray spectrum around the "π^0-bump," Astron. Astrophys. **615**, A108 (2018).

[9] I. M. Harrus, J. P. Hughes, and D. J. Helfand, Discovery of an X-ray synchrotron nebula associated with the radio pulsar PSR B1853 + 01 in the supernova remnant W44, Astrophys. J. **464**, L161 (1996).

[10] J. L. Caswell, J. D. Murray, R. S. Roger *et al.*, Neutral hydrogen absorption measurements yielding kinematic distances for 42 continuum sources in the Galactic plane, Astron. Astrophys. **45**, 239 (1975), https://ui.adsabs.harvard.edu/abs/1975A%26A....45..239C/abstract.

[11] I. M. Hoffman, W. M. Goss, C. L. Brogan, and M. J. Claussen, The OH (1720 MHz) supernova remnant masers in W44: MERLIN and VLBA polarization observations, Astrophys. J. **627**, 803 (2005).

[12] S. J. Sturner and C. D. Dermer, Association of unidentified, low latitude EGRET sources with supernova remnants, Astron. Astrophys. **293**, L17 (1995).

[13] V. Zabalza, NAIMA: A Python package for inference of relativistic particle energy distributions from observed nonthermal spectra, *Proceedings of the International Cosmic Ray Conference 2015* (2015), 922, arXiv:1509.03319.

[14] A. A. Abdo, M. Ackermann, M. Ajello *et al.*, Gamma-ray emission from the shell of supernova remnant W44 revealed by the Fermi LAT, Science **327**, 1103 (2010).

[15] R. Petre, K. D. Kuntz, and R. L. Shelton, The X-ray structure and spectrum of the pulsar wind nebula surrounding PSR B1853 + 01 in W44, Astrophys. J. **579**, 404 (2002).

[16] D. A. Smith, S. Abdollahi, M. Ajello *et al.*, The third Fermi Large Area Telescope catalog of gamma-ray pulsars, Astrophys. J. **958**, 191 (2023).

[17] V. L. Ginzburg and S. I. Syrovatskii, *The Origin of Cosmic Rays* (1964), https://ui.adsabs.harvard.edu/abs/1964ocr..book.....G/exportcitation.

[18] R. J. Gould, Energy loss of a relativistic ion in a plasma, Physica **58**, 379 (1972).

[19] T. Siegert, J. Berteaud, F. Calore, P. D. Serpico, and C. Weinberger, Diffuse galactic emission spectrum between 0.5 and 8.0 MeV, Astron. Astrophys. **660**, A130 (2022).

[20] A. E. Vladimirov, S. W. Digel, G. Jóhannesson, P. F. Michelson, I. V. Moskalenko, P. L. Nolan, E. Orlando, T. A. Porter, and A. W. Strong, GALPROP WebRun: An internet-based service for calculating galactic cosmic ray propagation and associated photon emissions, Comput. Phys. Commun. **182**, 1156 (2011).

[21] Fermi LAT Collaboration, Galactic interstellar emission model for the 4fgl catalog analysis, open document (2019), https://fermi.gsfc.nasa.gov/ssc/data/analysis/software/aux/4fgl/Galactic_Diffuse_Emission_Model_for_the_4FGL_Catalog_Analysis.pdf.

[22] https://fermi.gsfc.nasa.gov/ssc/data/access/lat/BackgroundModels.html.

[23] https://github.com/fermi-lat/Fermitools-conda/.

[24] J. A. Tomsick, S. E. Boggs, A. Zoglauer *et al.*, The Compton spectrometer and imager, Proc. Sci. ICRC2023 (**2023**) 745.

[25] O. Adriani, G. C. Barbarino, G. A. Bazilevskaya *et al.*, An anomalous positron abundance in cosmic rays with energies 1.5–100 GeV, Nature (London) **458**, 607 (2009).

[26] J. Chang, J. H. Adams, H. S. Ahn *et al.*, An excess of cosmic ray electrons at energies of 300–800 GeV, Nature (London) **456**, 362 (2008).

[27] M. Aguilar, D. Aisa, A. Alvino *et al.*, Electron and positron fluxes in primary cosmic rays measured with the Alpha Magnetic Spectrometer on the International Space Station, Phys. Rev. Lett. **113**, 121102 (2014).

[28] DAMPE Collaboration, Direct detection of a break in the teraelectronvolt cosmic-ray spectrum of electrons and positrons, Nature (London) **552**, 63 (2017).

[29] M. A. Malkov, P. H. Diamond, and R. Z. Sagdeev, On the mechanism for breaks in the cosmic ray spectrum, Phys. Plasmas **19**, 082901 (2012).

[30] J. McEnery, A. van der Horst, A. Dominguez *et al.*, All-sky medium energy gamma-ray observatory: Exploring the extreme multimessenger universe, Bull. Am. Astron. Soc. **51**, 245 (2019), https://ui.adsabs.harvard.edu/abs/2019BAAS...51g.245M.

[31] B. Liu, R.-z. Yang, and F. Aharonian, Nuclear de-excitation lines as a probe of low-energy cosmic rays, Astron. Astrophys. **646**, A149 (2021).

[32] B. Liu, R.-z. Yang, X.-y. He, and F. Aharonian, New estimation of the nuclear de-excitation line emission from the supernova remnant Cassiopeia A, Mon. Not. R. Astron. Soc. **524**, 5248 (2023).

[33] A. M. Hillas, The origin of ultra-high-energy cosmic rays, Annu. Rev. Astron. Astrophys. **22**, 425 (1984).

[34] K. Kotera and A. V. Olinto, The astrophysics of ultrahigh-energy cosmic rays, Annu. Rev. Astron. Astrophys. **49**, 119 (2011).

[35] C. D. Dermer and A. Atoyan, Ultra-high energy cosmic rays, cascade gamma rays, and high-energy neutrinos from gamma-ray bursts, New J. Phys. **8**, 122 (2006).